Amplitude and phase recovering from a micro-digital hologram using angular spectrum

M. León*, R. Rodríguez-Vera, J.A. Rayas, and S. Calixto

Centro de investigaciones en óptica,
A.C. Loma del bosque 115, León, Guanajuato, 37150, México,
e-mails:*migue@cio.mx; rarove@cio.mx; jrayas@cio.mx; scalixto@cio.mx

In this paper we present a method to get the complex amplitude of a digital hologram obtained through phase shifting transmission digital holographic microscopy. This is based on the angular spectrum method as a reconstruction algorithm employing an in-line experimental setup. The reconstruction technique automatically eliminates the zero order and the twin images from the digital hologram. By means of a reference hologram reconstruction method, a temporal averaging procedure and a focus distance averaging of the reconstructed complex amplitude, we extend an already efficient methodology to obtain high precision phase images with a reduced amount of aberrations caused by the microscope objective, and at the same time, we reduce the optical noise of the reconstructed complex amplitude. Using a homemade micro-thin film step surface, our system was calibrated and made traceable to an atomic force microscope (AFM). It is shown that our experimental results, compared to those given by the AFM, reach an axial accuracy of 9.7 nm from a typical phase sample.

Keywords: Digital holography; aberration compensation; computer holography; phase retrieval; microscopy; image reconstruction techniques; phase measurement; surface measurements; roughness.

En este trabajo presentamos una metodología para la obtención de la amplitud compleja de un holograma digital por medio de un microscopio holográfico digital en transmisión usando corrimiento de fase. Como método de reconstrucción se usa el algoritmo de propagación del espectro angular, empleando un arreglo experimental en eje. Esta técnica de reconstrucción elimina de manera automática el orden cero y la imagen gemela del holograma digital. Por medio del método de reconstrucción del holograma de referencia, el método del promediado temporal y el método de promediado de la distancia focal de la amplitud compleja reconstruida ampliamos una metodología eficiente para obtener imágenes de fase de alta precisión con una cantidad reducida de aberraciones provocadas por el objetivo de microscopio, así como la reducción de ruido óptico de la amplitud compleja reconstruida. Usando una micro película delgada superficial en forma de escalón hecha en casa como primera muestra, nuestro sistema fue calibrado y con los resultados de un microscopio de fuerza atómica como medio de trazabilidad de la misma muestra. Se muestra que nuestros resultados experimentales comparados con los del microscopio de fuerza atómica alcanzan una precisión axial de 9.7 nm de una muestra típica de fase.

Descriptores: Holografía digital; compensación de aberraciones; holografía por computadora; recuperación de fase; microscopia; técnicas de reconstrucción de imagen; medición de fase; medición superficial; rugosidad.

PACS: 42.15.Fr; 61.05.jp; 07.60.Pb; 42.30.Wb.

1. Introduction

Digital holographic microscopy (DHM) is a powerful tool for the study of microscopic samples through the retrieval of amplitude and phase from a wavefront reflected or transmitted through it. Phase reconstruction is of particular interest since it allows surface topography measurements at a microscopic scale for the lateral dimension, while for the axial dimension, it is at a sub-wavelength scale. Several methods have been proposed to obtain amplitude and phase measurements in DHM [1-16]. Fresnel's integral method is typically used in order to reconstruct a continuous field of the object's complex amplitude at the off-axis hologram plane [1,8,17-22]. However, it takes a longer execution time, has reconstruction distance restrictions, and is less accurate than the angular spectrum method [23, 24]. On the other hand, in-line configurations achieve the highest lateral resolutions, less speckle noise and higher accuracy, in comparison to off-axis experimental setups [25-27]. Off-axis and in-line digital holography, in tandem with phase shifting, allow the suppression of the diffracted zero order and the twin image [11,18,21,27];

in addition, free of these terms, the object's amplitude and phase are obtained. Off-axis digital holography limits the reconstruction due to the bandwidth of the object, which can be overtaken by using in-line setup [25-27,28]. Any imaging optical system bears quality image, characterized by its aberrations. DHM is not the exception, since it uses a microscope objective in order to image the specimen under test; this problem has been overcome using specialized software and setups to remove the wavefront aberrations [29-33].

By means of spatial and temporal averaging, we present the experimental results applied to a SiO_2 thin film of 78 nm in height. Applying the reference hologram method [11,33,34], we correct the optical aberrations induced by the microscope objective, in addition to the ruggedness and non-planarity of the object. To reduce shot-noise, we apply an average of several holograms taken in an interval of time. Finally, we propose the averaging of the topographical maps at different reconstruction distances with the purpose of improving axial accuracy. For the measurement of phase-contrast imaging quality we use spatial standard deviation. A
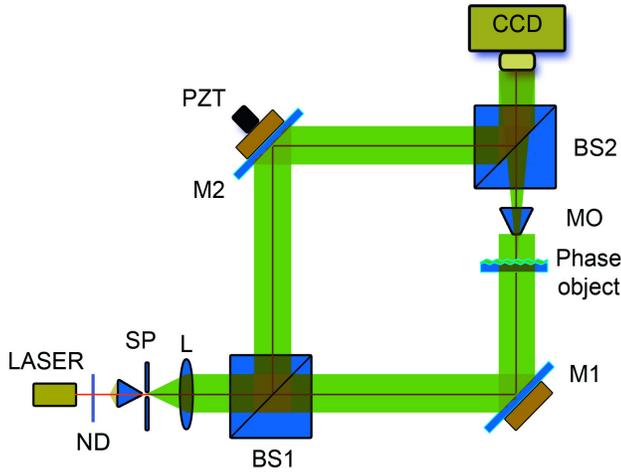
FIGURE 1. In-line transmission holographic microscope imaging scheme. BS, beam splitter; L, lens; MO, microscope objective; SP, spatial filter; ND, neutral density filter, M, mirror, PZT, piezo-transducer.

typical phase sample was made to test the axial phase resolution of our system without having to use a sample with very high optical performance, as J. Woong and C. Ki, to reduce the object's optical noise [11]. As illumination source we use a linelly polarized laser diode at 532 nm, thus getting a simpler set up than that used by J. Kühn, *et.al.*, who used two length waves of low coherence to eliminate optical noise and non-correlated noise coming from the object [33].

Our objective is to obtain the topographical measurement of a phase object from its refraction index. This proposal also employs phase shifting in order to have higher image quality and accuracy. This paper is divided in sections. Section 2 starts with a brief description of DHM and holographic reconstruction using the angular spectrum method. In the same section, the algorithm used to obtain the amplitude and phase from the phase shifting method, together with aberration compensation, is described; the phase to specimen height formula is shown in this section too. In Sec. 3, experimental results are shown. In our in-line DHM technique, the 78.00 nm step-wise specimen made of SiO_2 thin film is used as a calibrating gauge. To validate our methodology, an Atomic Force Microscope (AFM) was used as a traceable metrological aspect. Finally, the experimental results of the topographic measuring of an etched pattern on a photo resist are shown. These experimental results yielded a standard deviation of 9.7 nm.

2. Hologram reconstruction

We use transmission in-line configuration imaging for our implementation shown in Fig. 1. This setup is a modified Mach-Zehnder interferometer where a specimen is illuminated with a monochromatic plane wave that is propagating from an object plane $O(x, y)$ to a CCD camera $O(X, Y)$ plane, which we called object wave. To get a magnified image of the sample, and a high level of accuracy in the lateral
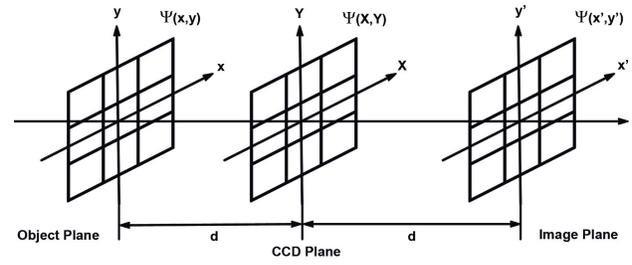
FIGURE 2. Illustration of the coordinate system of the diffraction theory.

resolution we used a microscope objective (MO) placed between the object and beam splitter BS2. The object wave transmitted by the specimen object is collected by the MO, and it is the propagated to the CCD camera plane. The reference wave $R(x, y)$ is another plane wave coming from beam splitter BS1. Both reference and object waves interfere on the CCD face plate, combined by beam splitter BS2. In this manner, an intensity interference pattern is registered by the CCD and given by

$$
\begin{aligned}
I(X, Y) &= |O(X, Y) + R(X, Y)|^2 \\
&= O^2(X, Y) + R^2(X, Y) \\
&\quad + O^*(X, Y)R(X, Y) + O(X, Y)R^*(X, Y), \quad (1)
\end{aligned}
$$

where the first two terms are the DC term, and the last ones represent the virtual and real image respectively, while $*$ denotes the conjugate complex.

In order to suppress the DC term and the virtual image term from Eq. (1), we employ the phase shifting method to calculate an initial phase $\phi_0(X, Y)$ and the initial amplitude object $A_0(X, Y)$ explained and described by Yamaguchi *et.al.* [18].

As a result, the object complex amplitude distribution at the (X, Y) plane is given by

$$
\begin{aligned}
h(X, Y) &= A_0(X, Y) \\
&\quad \times \exp[i * (\phi_0(X, Y) + \phi(X, Y))], \quad (2)
\end{aligned}
$$

where $\phi(X, Y)$ is the phase aberration term, induced by MO, mainly.

As illustrated in Fig. 2, $\Psi(X, Y)$ denotes the diffracted field from an object that falls within the CCD sensor. The complex amplitude of the reconstructed field can be given by the Rayleigh-Sommerfeld diffraction integral,

$$
\psi(x', y') = \int\limits_{-\infty}^{+\infty} \int [\psi(X, Y)\exp(ik\rho)/\rho] \, d\xi d\eta, \quad (3)
$$

where $\rho = (d^2 + (\xi - x')^2 - (\eta - y')^2)^{1/2}$, k is the wave vector magnitude, and d is the reconstruction distance. $\psi(x', y')$ can be equally yielded by the diffraction angular spectrum integral (ASI) through the spatial frequency domain, as follows [28]:

$$
\psi(x', y') = \Im^{-1} \{H(\alpha, \beta)T(\alpha, \beta)\}_{x',y'} \quad (4)
$$

where $H(\alpha, \beta)$ is the Fourier spectrum of the $h(X, Y)$, and $T(\alpha, \beta)$ is the transfer function of the free space propagation, which is given by

$$T(\alpha, \beta) = \exp[i\vec{k}d(1 - (\alpha\lambda)^2 - (\beta\lambda)^2)^{1/2}], \quad (5)$$

where λ is the wavelength.

The digital hologram $h(k, l)$ results from the two dimensional spatial sampling of $h(X, Y)$ by the CCD as follows:

$$h(k, l) = H(X, Y)rect(X/L, Y/L)$$

$$\times \sum_k^N \sum_l^N \delta(X - k\Delta X, Y - l\Delta Y) \quad (6)$$

where k and l are integers $(-N/2 \leq k, l \geq N/2)$, and $\Delta X = \Delta Y$ are the pixel size or sampling intervals in the hologram plane; $L = N\Delta X$, N is the pixel number.

In practice, FFT is employed to calculate the Fourier spectrum of $h(k, l)$, and the discrete form of $T(\alpha, \beta)$ is as follows:

$$T(\xi, \eta) = \exp \left[\begin{array}{c} i\vec{k}d(1 - (\lambda[\xi - (N/2)])^2 \\ -(\lambda[\eta - (N/2)])^2)^{1/2} \end{array} \right] \quad (7)$$

where ξ and η are integers $(-N/2 \leq \xi, \eta \geq N/2)$ in the discrete frequency domain.

Now, Eq. (4) can be represented in a discrete form as:

$$\psi(m, n) = IFFT[FFT(h(k, l)) \times T(\xi, \eta)] \quad (8)$$

As the MO produces a curvature of the wave front on the object arm, this phase aberration must be corrected. $h(k, l)$ has to be multiplied by a reference conjugated hologram $\Gamma'(k, l)$ directly at the hologram plane, which corrects aberrations and image distortions defined by Tristan Colomb *et al.* [33,34] as

$$\Gamma'(k, l) = |R(k, l)^*|^{-1} |O(k, l)|^{-1} \exp[-i\phi(k, l)], \quad (9)$$

where $|O(k, l)|$ is the amplitude of the object wave with an optical flat as specimen in the system, $\phi(k, l)$ is the phase aberration function of the system during calibration, and appears with a negative sign in order to cancel the system phase aberration in the actual measurement. For a detailed explanation of the procedure, see Ref. 33.

The reconstructed wave front, Eq. (8), then become

$$\psi(m, n) = IFFT \left[\begin{array}{c} FFT(\Gamma'(k, l)h(k, l)) \\ \times T(\xi, \eta) \end{array} \right]. \quad (10)$$

That is, a mathematical model to digital hologram reconstruction using ASI.

Since $\psi(m, n)$ is an array of complex numbers, we can obtain the amplitude image by calculating the intensity,

$$Int(m, n) = Re[(\psi(m, n))^2] + Im[(\psi(m, n))^2], \quad (11)$$

and the phase image by calculating the argument,

$$\phi(m, n) = \tan^{-1}\{Im[\psi(m, n)]/Re[\psi(m, n)]\}. \quad (12)$$
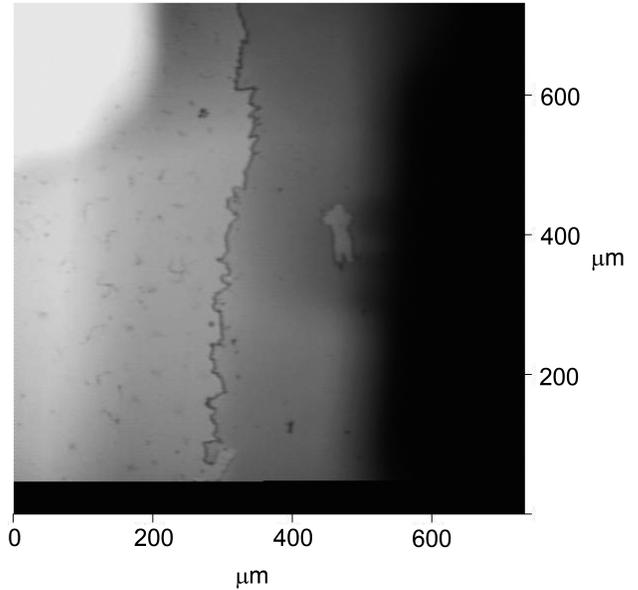
FIGURE 3. Photography of the step constructed with a SiO_2 coating on a glass substrate. I can be noticed the irregular frontier of the step, where the right side is the coating region.

Another important fact is the physical thickness of the specimen, which is given by the phase to specimen height formula

$$h = [\lambda(\Delta\phi/2\pi)/(n - n_0)], \quad (13)$$

where λ is the wavelength, $\Delta\phi$ is the phase step, and $(n - n_0)$ is the index difference between the specimen material and air.

3. Experimental results

In this section, the experimental results obtained from DHM to get high accuracy in topographic measurements of an object's surface are presented. We used an in-line transmission holographic Mach-Zehnder interferometer, as it is shown in Fig. 1. A 40X, NA = 0.65 microscope objective was employed, in addition to a Pixelink CCD camera that captures 1280×1024 pix images with a 6.7×6.7 μm pixel size. Additionally, a mirror attached to a piezoelectric transducer (PZT) controlled by a computer, for phase shifting, was included in the same arrangement. As a coherent illumination source, a linearly polarized laser diode of 532 nm wavelength and 50 mW was employed.

First, a 78 nm step-wise specimen made of SiO_2 thin film was used as a calibrating gauge with a refraction index of 1.4600. A micro-photograph is shown in Fig. 3. To ensure a real and accuracy measurement reference, it was analyzed with a Digital Instruments 3100 AFM, with max. scan area of 100 μm horizontal x 100 μm vertical x 7 μm high, and we extracted a measured profile. Figure 4 presents the results from the AFM. The sample was not uniform and very dirty, due to the fact that the sample had been made at home using a Balzer B-510vapor deposition machine. However, the following results contain an object-dependent 'bias', although the measurements should be interpreted in terms of noise
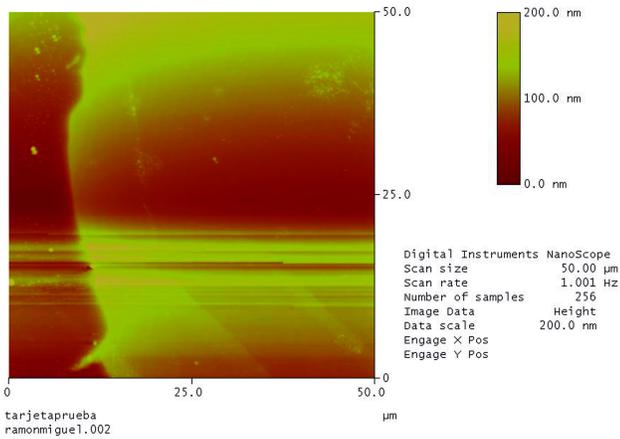
FIGURE 4. Topographic measurement done by a 3100 AFM of Digital Instruments with max. scan area of 100 μm horizontal x 100 μm vertical $\times$ 7 μm high, from a SiO$_2$ coating step on a glass substrate.
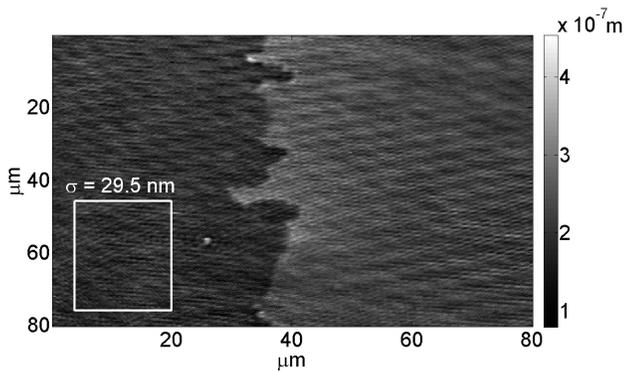
FIGURE 5. Reconstructed phase image from a reference hologram and the SiO$_2$ step sample hologram.

reduction, not absolute values converging to zero. We got a good measurement reference to compare the results by DHM.

For the reconstruction algorithm process, four shifted holograms were taken of the flat area near the step to get the complex amplitude of the reference hologram expressed in Eq. (2). Next, we got the complex amplitude of the SiO$_2$ step sample, in a fashion similar to how the reference hologram was obtained. Once both the complex amplitude reference hologram and the SiO$_2$ step sample were calculated, the wave field was reconstructed, as expressed by Eq. (10). The reconstructed phase is presented in Fig. 5. Every SiO$_2$ step sample phase image shown in this paper has been inverted to render topographic phase images.

As we can see in Fig. 5, the step is blurred by remaining noise for many reasons, such as some non-compensated aberrations, shot noise, parasitic interferences, or signal-to-noise ratio differences due to degradation of the interference regimes. In the zone delimited by the white square, the noise measured by standard deviation is σ=29.5 nm, which represents the usual parameters to estimate DHM axial accuracy [35].

As it is well known, shot noise contribution in DHM needs to be accounted for in our optical system [34]. To remove this contribution of the phase noise, a temporal averaging over a short period of time is applied by acquiring a sequence of 15 complex amplitudes of the reference hologram and the sample test, and then, each wavefront is averaged before propagation, to get a detailed explanation see Ref. 33 and 34.

In Fig. 6, one can see the improved phase image compared to the phase image before time averaging in Fig. 5. The improvement was of 53% for the standard deviation, which is adjusted with the theoretical and experimental aspects [34,35].

3.1. Focus distance averaging

In order to get a better phase image, we propose an averaging of the reconstructed complex amplitude obtained when applying Eq. (10) in an interval of reconstruction distance d. Let us assume that these wavefronts are not correlated in certain degree each one of them, and they have similar topographic standard deviations. In our case, this interval in the reconstruction distance is between shortly before obtaining a focused wave front (df) and shortly after (-100 μm$< df < +100$ μm). Figure 7 a) shows a focused amplitude image, while Fig. 7 b) shows a defocused amplitude image. We averaged 20 phase images obtained from the reconstructed amplitude at reconstruction distances df=-100 μm at +100μm with increments of 10μm; in Fig. 8, one can see a 30% improvement in the phase topographical map as compared with the phase image in Fig. 6. The resulting spatial standard deviation in Fig. 8 is σ = 9.7 nm in the zone delimited by the white square. The measuring zone was chosen as a cleaner, more uniform and closer place from the profile measurement. The results contain an object-dependent 'bias' due to the roughness and dirtiness of the sample, but the measurements should be interpreted in terms of noise reduction, not absolute values converging to zero, as commented above.
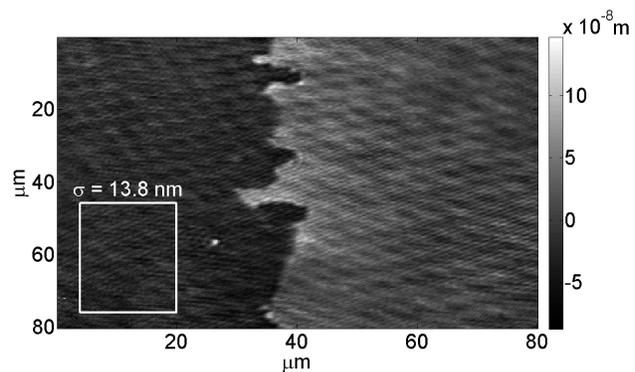
FIGURE 6. Temporal averaging sequence with an improved phase image.
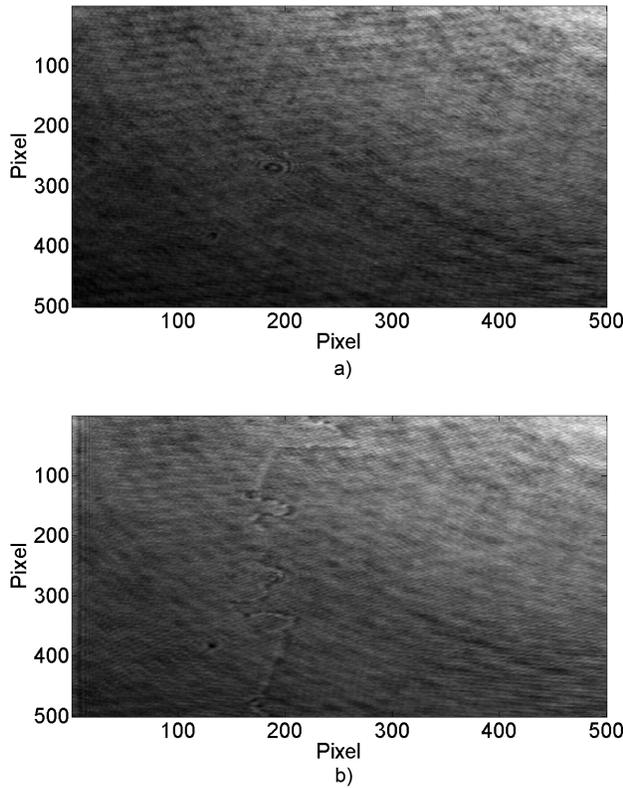
FIGURE 7. Image from the reconstructed amplitude at different reconstruction distances. a) Focused amplitude image at df=0 μm; b) Defocused amplitude image at df=-100 μm.
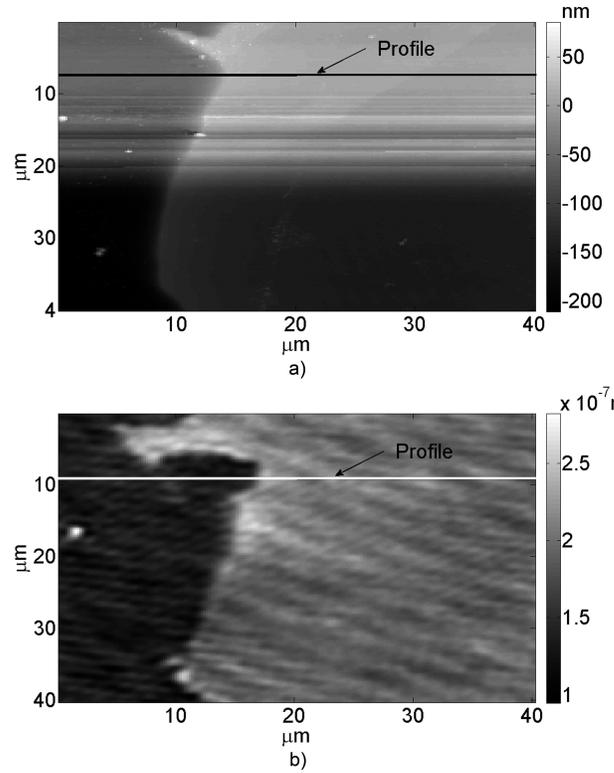
FIGURE 9. Profiles taken from the similar zone in both techniques by AFM and DHM.
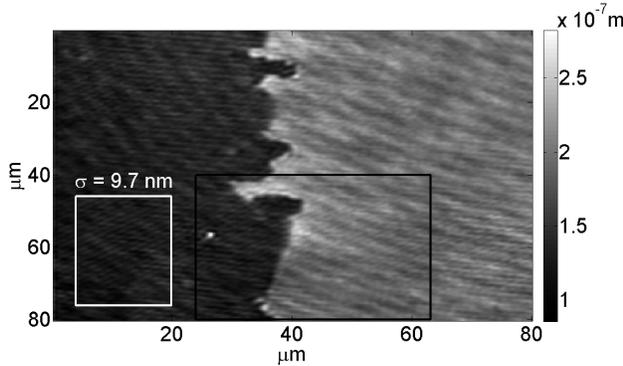
FIGURE 8. Phase image improved by focus distance averaging.
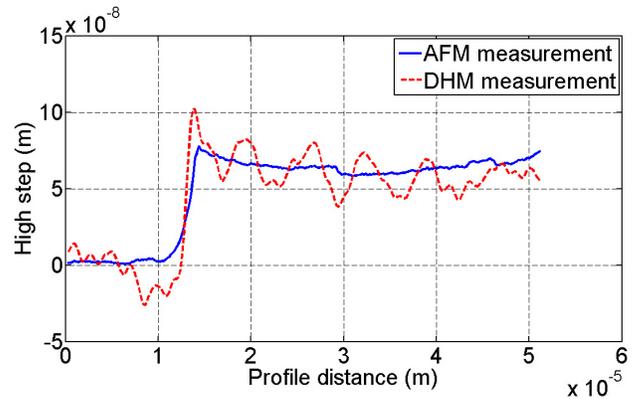
FIGURE 10. Profiles height measured with AFM and DHM techniques. These graphs are extracted from the lines show in Figs. 9a) and 9b), respectively.

Finally, Fig. 10 presents the profiles extracted from a similar zone of the measurement done by AFM and by DHM. One can see the similar zone where the profiles were taken; in Fig. 9 a) there is a topographical measurement done by AFM, while Fig. 9 b) is the section delimited by the black square of the phase image in Fig. 8. These profiles give heights measured from the lines shown in Figs. 9 a) and 9 b). One can notice a slight difference between the AFM measured profile and DHM; this difference represents the parasitic remaining interferences from the sample substrate. This noise can be reduced by using a short coherence source instead of a coherent light source, as cited by T. Colomb *et al.* [33]. However, based on the thin step measured heights in Fig. 10, we can es-

timate the profile average by AFM as 64.5 nm high, while the profile average by DHM as 61.7 nm high. After comparing both measurements, we find a difference of only 2.8 nm.

Once the system was calibrated, we analyzed the surface topography of a layer of photo resist deposited on a glass substrate and etched by a chemical process. A thin and uniform layer of photo resist was deposited on a glass substrate for the spinning method. Later, we placed an Edmund NBS 1963 A resolution card in front of the photo resist layer, to use it as mask. Later, we illuminated the arrangement vertically with a plane wavefront of 432 nm (to which the photo resistst is
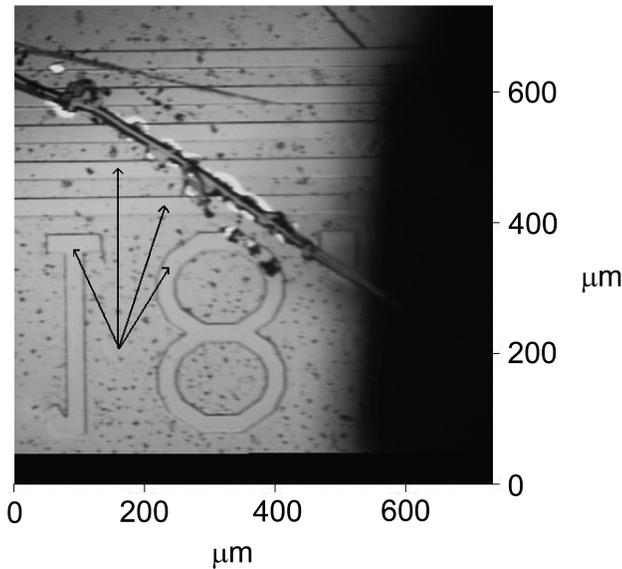
FIGURE 11. Photography of etch on photoresist. The numbers and similar lines exhibited by arrows have the photoresist film step.
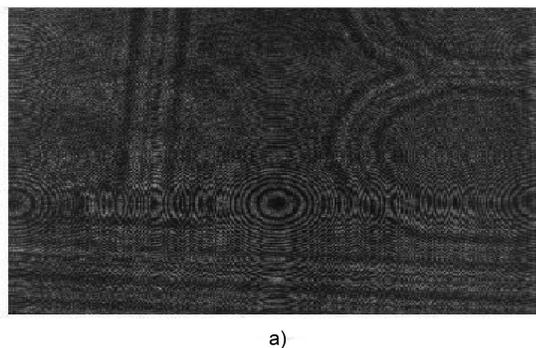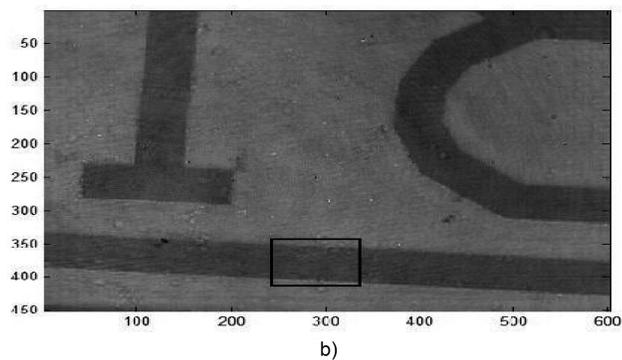
FIGURE 12. .a) Digital hologram from the sample test made in home. b) Reconstructed phase image applying the methodology above described.

sensitive) for a short period of time (1.5 sec). Once the exposition to radiation had taken place, we proceeded to reveal and fix the pattern on the photo resist layer. For a detailed description of the process, see Ref. 36.

In Fig. 11 we show a photograph of the specimen where the refractive index of the photo resist is 1.52, which was measured using an Abbe refractometer after the process of etching had ended.
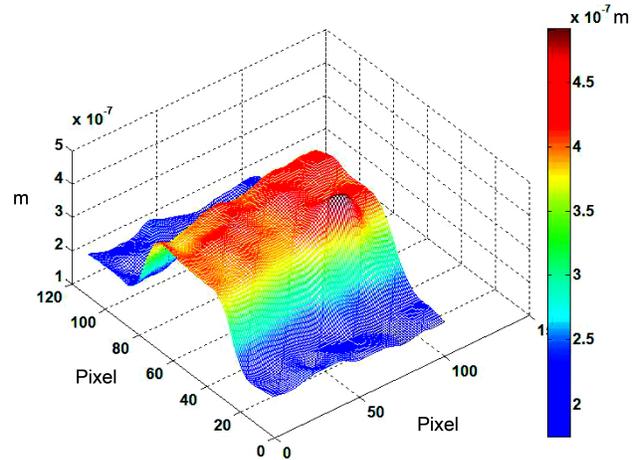
FIGURE 13. 3D topography of the photoresist etched image took from the square of the phase image in Fig. 12 b).
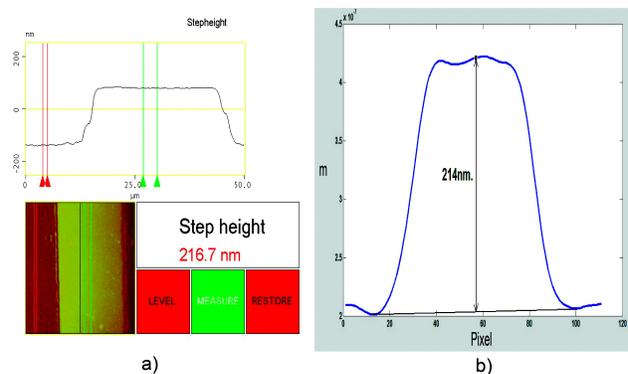
FIGURE 14. a) Groove measured with AFM. b) Groove measured with proposed methodology.

Applying the proposed methodology, we recorded the hologram and applied the reconstruction algorithm. Fig. 12 a) presents a digital hologram, and Fig. 12 b) shows its reconstructed phase image.

Figure 13 shows the 3D topography image taken from the black square of the phase image in Fig. 12 b), where the surface measurement was taken. In Fig. 14 a) we have the measurement made with the AFM; an average height of 216.7 nm was obtained. In turn, Fig. 14 b) shows the same groove, where we can measure an average eight of 214 nm. By comparing both measurements, we find a difference of only 2.77 nm. It is in agreement with the predicted value obtained in the previous calibrating stage.

4. Conclusions

In this paper we describe an in-line transmission DHM for measuring topography of a phase specimen. We combine the angular spectrum reconstruction algorithm, phase shifting and aberration compensation using the reference hologram, all in one, in order to have the amplitude and phase of the specimen. With this algorithm, the DC term, or zero order, and the twin holographic image are removed; as a result, high

quality holographic reconstruction is obtained. The proposed method was used to measure the topography of a phase specimen. The DHM experimental setup was calibrated using a step-wise sample of 78 nm in height; this step-wise specimen was made of SiO_2 thin film. To achieve high axial resolution in the phase image, we applied a reference hologram to correct parasitic phase aberrations. To eliminate the shot noise that is typical of this optical set up, we employed temporal averaging of the reference hologram and the sample. Finally, in order to reduce the noise gain, we propose a different spatial averaging of the reconstruction distance, gaining an advantage of 30% in noise reduction in the phase image. The axial accuracy results, compared to the AFM measurements, are in agreement in axial measurement. The measurements obtained yield a standard deviation of 11.1 nm in depth for a 100×100 μm field of view, with the possibility of improving the axial accuracy using short coherence light as the source of illumination. This methodology should be useful for studying biological structures and MEMS.

Acknowledgments

1. E. Cuche, P. Marquet, and C. Depeursinge, *Appl. Opt.* **38** (1999) 6994.

2. G. Pedrini, P. Fröning, H. Tiziani, and F. Santoyo, *Opt. Comm.* **164** (1999) 257.

3. Y. Takaki and H. Ohzu, *Appl. Opt.* **38** (1999) 2204.

4. Y. Takaki, H. Kawai, and H. Ohzu, *Appl. Opt.* **38** (1999) 4990.

5. M.K. Kim, *Opt. Exp.* **7** (2000) 305.

6. G. Pedrini, S. Schedin, and H. Tiziani, *J. Mod. Opt.* **47** (2000) 1447.

7. L. Xu, X. Peng, A. Asundi, and J. Miao, *Opt. Eng.* **40** (2001) 2533.

8. V. Kebbel, H.J. Hartmann, and W. Jüptner, *Proc. SPIE* **4398** (2001) 189.

9. L. Xu, X. Peng, J. Miao, and A.K. Asundi, *Appl. Opt.* **40** (2001) 5046.

10. F. Dubois *et al.*, *Appl. Opt.* **41** (2002) 4108.

11. J. Woong and C. Ki, *Opt. Eng.* **46** (2007) 040506-1.

12. D. Panah, Mehdi, and J. Bahram, *Opt. Exp.* (2007) 10761.

13. M. Paturzo *et al.*, *Opt. Exp.* **16** (2008) 17107.

14. V.R. Singh, A. Asundi, *Opt. Exp.* **17** (2009) 8220.

15. A. Arun and J. Bahram, *Opt. Lett.* **35** (2010) 766.

16. M. Kanka, A. Wuttig, C. Graulig, and R. Riesenberg, *Opt. Lett.* **35** (2010) 217.

17. U. Schnars and W. Jüptner, *Appl. Opt.* **33** (1994) 179.

18. I. Yamaguchi and T. Zhang, *Op. Lett.* **22** (1997) 1268.

19. E. Cuche, F. Bevilacqua, and C. Depeursinge, *Opt. Lett.* **24** (1999) 291.

20. E. Cuche, P. Marquet, and C. Depeursinge, *Appl. Opt.* **39** (2000) 4070.

21. S. De Nicola, P. Ferraro, and A. Finizio, *Op. & La. in Eng.* **37** (2002) 331.

22. T. Kreis, *Opt. Eng.* **41** (2002) 771.

23. M. Kim, L. Yu, and C.J. Mann, *"Digital holography and multi-wavelength interference techniques", in "Digital holography and Three dimensional display: Principles and applications"* (Ting-Chung Poon, Springer, 2006). pp. 51-93.

24. C. Liu, D. Wang, and Y. Zhang, *Op. Eng.* **48** (2009) 1058021.

25. L. Xu, J. Miau, and A. Asundi, *Op. Eng.* **39** (2000) 3214.

26. H. Jin, H. Wan, Y. Zhang, Y. Li, and P. Qiu, *J. Mod. Opt.* **55** (2008) 2989.

27. D.P. Kelly, B.M. Hennelly, N. Pandey, T.J. Naughton, and W.T. Rodes, *Opt. Eng.* **48** (2009) 1.

28. J.W. Goodman, *Introduction to Fourier Optics* third ed., (Roberts & company Pub.2005).

29. S. De Nicola, P. Ferraro, and A. Finizio, *Op. & La. in Eng.* **37** (2002) 331.

30. T. Colomb, E. Cuche, F. Charrière, J. Kühn, and N. Aspert, *Appl. Op.* **45** (2006) 851.

31. W. Zhou, Y. yu, and A. Asundi, *Op. & La. in Eng.* **47** (2009) 264.

32. A. Nelleri, J. Joseph, and K. Singh, *Op. & La. in Eng.* **48** (2010) 27.

33. P. Ferraro *et al.*, *Appl. Opt.* **42** (2003) 1938.

34. J. kühn *et al.*, *Meas. Sci. Technol* **19** (2008) 1.

35. F. Charrière *et al.*, *Opt. Exp.* **15** (2007) 8818.

36. A. Martinez, *"Doctoral thesis", centro de investigaciones en óptica* (León, Guanajuato, México 2001).